Piezo-optic and elasto-optic effects in lead molibdate crystals

Piezo-optic and Elasto-optic Effects in Lead Molibdate Crystals

B. Mytsyk[1], N. Demyanyshyn[1], A. Sakharuk[1] and A. Erba[2]

[1]*Karpenko Physico-Mechanical Institute of NAS of Ukraine, 5 Naukova Street, 79060 Lviv, Ukraine*

[2]*Dipartimento di Chimica, Università di Torino, Via Giuria 5, 10125 Torino, Italy*

Piezo-optical and elasto-optical properties of lead molibdate ($PbMoO_4$) crystals are investigated, as determined by the quantum-mechanical *ab initio* calculation of the full set of photo-elastic, piezo-optic and elastic tensor components. Indicative surfaces are built, which describe the anisotropy of these stress- and strain-optical effects and allow for its rigorous analysis. Maximum values of these properties are determined as well as the geometries of acousto-optic interaction displaying the maximum efficiency. Lead molibdate crystals are found to be characterized by a large piezo-optic efficiency, the maximum change of the optical path (per unit of mechanical stress and specimen length) being calculated to 24.9 Br, which is a much larger value than previously reported for other well-known piezo-optic materials such as $LiNbO_3$, $CaWO_4$ and GaP. It is also shown that a significant rotation (up to several tens of degrees) of the optical indicatrix about the X_3 optical axis is induced by uniaxial pressure or deformation, depending on pressure (or deformation) direction rather than magnitude, which has relevant implications in the design of acousto-optic cells.

OCIS codes: (160.1050) Materials : Acousto-optical materials; (260.1180) Physical optics : Crystal optics

1. Introduction

Despite being a well-known acousto-optic material [1–3], lead molibdate ($PbMoO_4$) has not yet been thoroughly characterized in terms of its stress- and strain-optical features. For instance, large discrepancies are found between sets of its elasto-optic coefficients (ELOC) p_{in} as reported in the literature in different studies, which are the main physical parameters governing its acousto-optic efficiency. The value of the p_{11} coefficient has been reported to be 0.24 by Coquin *et al.* [2] and 0.28 by Gabrielyan *et al.* [4]; the p_{13} coefficient spans an even larger range, from 0.255 [2] to 0.35 [4] and 0.49 [5]; the values of the p_{61} coefficient differ by more than a factor of 4, from 0.013 [2] to 0.05 [4]. Apart from absolute values, signs of the ELOCs have not yet been determined, which makes it impossible to accurately describe the spatial anisotropy of the elasto-optic effect (ELOE) in $PbMoO_4$ crystals, as both absolute values and signs are obviously needed for this purpose [6,7]. Moreover, the piezo-optic effect (POE) in lead molibdate, which is an essential physical parameter in the determination of the efficiency of piezo-optic light modulators and photoelastic pressure (or mechanical stress) sensors [8–11], has not yet been studied.

The aim of this paper is two-fold: i) the determination of the full set of piezo-optic π_{im} and elasto-optic p_{in} coefficients of lead molibdate $PbMoO_4$ by use of a recently developed quantum-mechanical *ab initio* theoretical approach [12,13], based on the density-functional-theory (DFT) and on the Coupled-Perturbed-Hartree-Fock/Kohn-Sham (CPHF/KS) method for the evaluation of the dielectric tensor of crystalline materials, as implemented in a developmental version of the CRYSTAL14 program [14]; ii) the careful analysis of the anisotropy of both the piezo-optic and elasto-optic effects in lead molibdate. Indicative surfaces of the POE and ELOE are here built, their maximum and minimum values found, and the acousto-optic quality coefficients determined, starting from the full fourth-rank piezo-optic and elasto-optic tensors provided by the theoretical calculations.

It is shown that lead molibdate crystals exhibit a large piezo-optic efficiency with a maximum change of the optical path of 24.9 Br (per unit of mechanical stress and specimen length), which is a

larger value than in other piezo-optic materials such as $LiNbO_3$, $CaWO_4$ and GaP. The rotation of the optical indicatrix (and correspondingly of the direction along which light polarization occurs) is also found to depend considerably on the direction of an applied uniaxial pressure or strain. The angle between light polarization vector ***i*** and direction of uniaxial pressure ***m*** (or strain ***n***) can be as large as several tens of degrees, which is an effect to be accurately accounted for in designing acousto-optic cells [15].

2. Quantum-mechanical calculation of elastic, piezo-optic and elasto-optic coefficients

The elastic, photoelastic and piezo-optic fourth-rank tensors of $PbMoO_4$ have been computed by using the fully-automated procedures implemented into the CRYSTAL14 program [12,13,16]. The hybrid PBE0 functional is used [17], which is known to provide accurate strain-related properties of solids [18-19]. An atom-centered Gaussian-type function basis set has been adopted where oxygen atoms are described by an all-electron 8-411G(2d) basis [20] while pseudo-potentials are used to describe the core of lead [21] and molybdenum [22] atoms. The optimized equilibrium lattice parameters are a = 5.472 and c = 12.097 Å, with a ratio c/a = 2.211 and fractional coordinates of the symmetry-irreducible oxygen atom $x_O = 0.2316$, $y_O = 0.1091$ and $z_O = 0.0436$.

Lead molibdate crystals belong to the $4/m$ symmetry class of the $I4_1/a$ space group and thus have seven symmetry-independent components of the elastic stiffness and compliance tensors (C_{mn} being elastic stiffness and S_{nm} elastic compliance constants), and ten symmetry-independent components of the piezo-optic and elasto-optic tensors. The computed symmetry-irreducible elastic constants are reported in Table 1, where they are compared with available experimental determinations by Coquin *et al.* [2], Gabrielyan *et al.* [4], and Farley *et al.* [23].

Table 1. Coefficients of elastic stiffness C_{mn} (in 10^9 N/m^2 = 1GPa) and elastic compliance S_{nm} (in 10^{-12} m^2/N = 1 Brewster = 1 Br) for $PbMoO_4$ crystal.

C_{mn}	C_{11}	C_{12}	C_{13}	C_{33}	C_{44}	C_{66}	C_{16}
This work	112.14	67.94	51.35	94.09	27.14	38.31	–12.82
[2]	109.2	68.3	52.8	91.7	26.7	33.7	13.6
[4]	108.0	63.2	50.7	95.2	26.4	35.4	15.8
[23]	109.0	68.0	53.0	92.0	26.7	33.7	–14.0
S_{nm}	S_{11}	S_{12}	S_{13}	S_{33}	S_{44}	S_{66}	S_{16}
This work	18.07	–10.01	–4.40	15.43	36.85	32.39	9.39
[23]	21.0	–12.4	–4.9	16.6	37.5	40.6	13.5

The comparison presented in Table 1 demonstrates that almost all the calculated C_{mn} and S_{nm} elastic coefficients coincide with the corresponding experimental values with a high accuracy, with deviations between the two sets that never exceed 10%, which corresponds to the scattering of experimental data in papers [2,4,23]. Slightly larger differences between calculated and experimental values are observed only for the C_{16} and C_{66} coefficients (and correspondingly for S_{16} and S_{66}) with deviations in the range from 6 to 30% according to different sources.

It is worth mentioning that the sign of the C_{16} coefficient depends on the particular choice for the right-handed coordinate system. If right-handed crystal physics coordinate system X, Y, Z is chosen in such a way that the deviation of the magnetic axes from $+X$ and $+Y$ is counterclockwise, then the C_{16} coefficient will have negative sign [23]. According to this conventional orientation, the C_{16} elastic coefficient has been reported to be negative for all the 4 crystals with scheelite structure studied by Farley *et al.* [23]: $CaMoO_4$, $SrMoO_4$, $PbMoO_4$ and $CaWO_4$. Piezo-optic coefficients (POC) π_{im} and elasto-optic coefficients p_{in} have also been computed by assuming the same

coordinate system, so as to ensure consistency of all computed quantities. Computed values of these coefficients are given in Table 2, where elasto-optic ones are also compared with previous experimental determinations [2,4].

Table 2. Piezo-optic π_{im} (in 10^{-12} m^2/N = 1 Br) and elasto-optic p_{in} coefficients for $PbMoO_4$ crystals (light wavelength λ = 632.8 nm, T = 20ºC).

π_{im}	π_{11}	π_{12}	π_{13}	π_{31}	π_{33}	π_{44}	π_{45}	π_{16}	π_{61}	π_{66}
This work	0.480	1.361	1.737	0.036	3.340	1.806	0.184	–0.895	–0.241	1.509
p_{in}	p_{11}	p_{12}	p_{13}	p_{31}	p_{33}	p_{44}	p_{45}	p_{16}	p_{61}	p_{66}
This work	0.247	0.263	0.258	0.178	0.318	0.049	0.005	–0.023	–0.030	0.064
[2]	0.24	0.24	0.255	0.175	0.300	0.067	–0.01	0.017	0.013	0.05
[4]	0.28	0.28	0.35	0.14	0.28	–	–	– 0.01	0.05	0.04

The computed absolute values of the p_{in} coefficients in Table 2 are relatively close to the experimental ones reported by Coquin *et al.* [2] while they significantly differ from those by Gabrielyan *et al.* [4] overall. The main difference between experimental [2] and computed elasto-optic coefficients is again represented by the signs of some coefficients (p_{45}, p_{16} and p_{61}). Let us stress that signs in [2] correspond to a different choice of the orientation of the right-handed coordinate system (i.e. a rotation by 180º about the +Z axis of the coordinate system given in [23]). An explicit account of the dependence of rotating, shear or rotating-shear piezo-optic and elasto-optic coefficients π_{im} and p_{in} on the choice of right-handed coordinate systems is given in detail in [24]. In Table 2 we also report the first determination of the full set of piezo-optic coefficients of $PbMoO_4$.

3. Results analysis

On the basis of the full and consistent quantum-mechanical determination of all of the elastic, elasto-optic and piezo-optic coefficients reported in Tables 1 and 2, this section is devoted to the investigation of the maximum piezo-optic efficiency of lead molibdate, to the detailed analysis of its piezo-optic and elasto-optic effect anisotropy, and to the determination of the maximum values of the acousto-optic quality coefficient for $PbMoO_4$ crystals.

3.1. Change of optical path induced by mechanical pressure

Given that five piezo-optic coefficients π_{im} of lead molibdate are large (π_{12}, π_{13}, π_{44}, π_{66}, and especially π_{33}, whose value exceeds 3 Br), it is expected that also the optical path change $\delta\Delta_k$ under the action of a mechanical stress will be large, as well as the efficiency of photoelastic light modulation. The optical path changes $\delta\Delta_k$ can be computed from the following well-known equation [24,25]:

$$\delta\Delta_k = -\frac{1}{2}\pi_{im}\sigma_m d_k n_i^3 + S_{km}\sigma_m d_k (n_i - 1), \tag{1}$$

where σ_m is the mechanical stress value, d_k the specimen thickness, n_i the refractive index, and i, k, m indices denote light polarization, light propagation and uniaxial pressure action directions, respectively. Let us rewrite Eq. (1) so as to introduce the optical path change per mechanical stress unit and specimen length unit:

$$\frac{\delta\Delta_k}{\sigma_m d_k} = -\frac{1}{2}\pi_{im} n_i^3 + S_{km}(n_i - 1), \tag{2}$$

which is an important parameter in the evaluation of the efficiency of piezo-optic pressure sensors and piezo-optic modulators [8–11]. Let us evaluate the value (to be given in Br) of this quantity for the experiment conditions $m = 3$, $i = 3$, $k = 2$ that is, when the large π_{33} POC is acting:

$$\frac{\delta\Delta_2}{\sigma_3 d_2} = -\frac{1}{2}\pi_{33}n_3^3 + S_{23}(n_3 - 1) = -19{,}3\ (77{,}5\%) - 5{,}6\ (22{,}5\%) = -24{,}9\ \text{Br}. \qquad (3)$$

Here, we have taken into account that $S_{23} = S_{13}$, we have used S_{km} and π_{im} coefficients as computed in this work (see Tables 1 and 2), and we have used $n_1 = n_2 = n_o = 2.386$ and $n_3 = n_e = 2.262$ for $\lambda =$ 632.8 nm from [2]. The negative sign of the result in (3) implies that the optical path of the light beam passing through the specimen decreases under the action of a positive specimen tension σ_m. Percentage values within square brackets in (3) represent the piezo-optic (77.5%) and the elastic deformation (22.5%) contributions to the specimen optical path change in the direction of light propagation. Other $\delta\Delta_k/(\sigma_m d_k)$ values, due to the other large POCs π_{12} and π_{13} are considerably lower than the result in (3) being equal to -15,3 and -17,9 Br, with piezo-optic contributions of 60% and 66%, respectively.

Let us now find the value of $\delta\Delta_k/(\sigma_m d_k)$ for experiment conditions where the large rotating-shear coefficient π_{66} is acting. In this case, Eq. (1) would become more complicated [24] as it involves summations of some π_{im} POC and S_{nm} coefficients. For these conditions ($m = 6$, $i = 6$ and $k = \bar{6}$, where direction $\bar{6}$ is a diagonal direction between axes $+X$ and $-Y$) we obtain:

$$\frac{\delta\Delta_{\bar{6}}}{\sigma_6 d_{\bar{6}}} = -\frac{1}{4}(\pi_{11} + \pi_{12} + \pi_{66})n_1^3 + \frac{1}{4}(2S_{11} + 2S_{12} - S_{66})(n_1 - 1) = -11{,}4(67\%) - 5{,}6(33\%) = -17{,}0\ \text{Br}. \qquad (4)$$

An even more complicated equation should be used for those conditions where the large rotating-shear coefficient π_{44} is involved. We shall not report this equation here as the corresponding $\delta\Delta_k/(\sigma_m d_k)$ value we find (-18.5 Br) is considerably lower than the result in (3). If the experiment conditions $m = 1$, $i = 3$, $k = 2$ are considered for which the lowest piezo-optic coefficient $\pi_{31} = 0{,}036$ Br is acting, then the optical path change will be:

$$\frac{\delta\Delta_2}{\sigma_1 d_2} = -\frac{1}{2}\pi_{31}n_3^3 + S_{21}(n_3 - 1) = -0{,}2(1{,}3\%) - 15{,}6(98{,}7\%) = -15{,}8\ \text{Br}. \qquad (5)$$

From the analysis reported above, it is rather clear that, whenever a large piezo-optic coefficient (such as π_{33}, π_{66} , π_{12}, π_{13}, π_{44}) is involved in the definition of the optical path change, the overall piezo-optic contribution is found to be much larger (up to 3.5 times) than the elastic deformation one (see Eqs. (3) and (4)). Eq. (5) refers to a qualitatively different case where the optical path change is almost entirely due to the elastic contribution, if one considers that the usual experimental error in the determination of $\delta\Delta_k$ is about 10%. Thus, this is a rare case of an "imaginary" POE.

To summarize, the result reported in (3) represents the largest value (24.9 Br) of the piezo-optic effect in $PbMoO_4$ crystals for light modulation. For comparison, the largest values of $\delta\Delta_k/(\sigma_m d_k)$ reported in the literature so far are 14 Br for lithium niobate [26], 13 Br for calcium tungstate [27], while the only known acousto-optic material with a comparable high value for this parameter is gallium phosphide, GaP, with 20 Br [28]. Thus, $PbMoO_4$ crystals should be considered as the best photoelastic materials on the basis of both the absolute value of the π_{33} piezo-optic coefficient and the large value of the corresponding optical path change $\delta\Delta_k$.

It is worth mentioning that the $\delta\Delta_k$ parameter can be transformed into the half-wave stress σ_{im} (referring to a cubic crystal specimen with the edge of 1 cm) or control stress $\sigma^o_{im} = \sigma_{im} d_k$, which are very useful parameters for engineering calculations. A half-wave mechanical stress with a value $\sigma_m = \sigma_{im}$ changes the optical path by $\lambda/2$. Correspondingly, by substituting in Eq. (3) σ_3 with σ_{33} and $\delta\Delta_2$ with $\lambda/2$, we get:

$$\frac{\lambda}{2\sigma_{33}d_2} = \frac{\lambda}{2\sigma^o_{33}} = -24{,}9\ \text{Br}, \qquad (6)$$

from which we can find the value of the control stress $|\sigma_{33}^{o}| = \lambda/(2\cdot 24{,}9\ \text{Br}) = 13{,}0$ êg/cm, which changes the intensity of the light passing through the specimen placed in the single pass interferometer arm, from $I = 0$ to $I = I_{max}$.

3.2. Piezo-optic effect anisotropy

The POE anisotropy is generally described by indicative surfaces (IS) of this effect [6, 7, 15]. The general equation for these ISs for crystals belonging to the 4/*m* symmetry class (in spherical coordinates) takes the following form [7]:

$$\begin{aligned}\pi'_{im}(\theta_i,\varphi_i,\theta_m,\varphi_m) = {} & (\pi_{11}\sin^2\theta_m\cos^2\varphi_m + \pi_{12}\sin^2\theta_m\sin^2\varphi_m + \pi_{13}\cos^2\theta_m + \frac{1}{2}\pi_{16}\sin^2\theta_m\sin 2\varphi_m)\sin^2\theta_i \times \\ & \times\cos^2\varphi_i + (\pi_{12}\sin^2\theta_m\cos^2\varphi_m + \pi_{11}\sin^2\theta_m\sin^2\varphi_m + \pi_{13}\cos^2\theta_m - \frac{1}{2}\pi_{16}\sin^2\theta_m\sin 2\varphi_m)\sin^2\theta_i\sin^2\varphi_i + \\ & + (\pi_{31}\sin^2\theta_m + \pi_{33}\cos^2\theta_m)\cos^2\theta_i + \frac{1}{2}[(\pi_{44}\sin\varphi_m + \pi_{45}\cos\varphi_m)\sin\varphi_i + (\pi_{44}\cos\varphi_m - \pi_{45}\sin\varphi_m)\cos\varphi_i]\times \\ & \times\sin 2\theta_m\sin 2\theta_i + (\pi_{61}\cos 2\varphi_m + \frac{1}{2}\pi_{66}\sin 2\varphi_m)\sin^2\theta_m\sin^2\theta_i\sin 2\varphi_i,\end{aligned} \tag{7}$$

where θ is the angle between the polarization direction of light ***i*** (or direction of uniaxial pressure ***m***) and the X_3 axis, and φ is the angle between the polarization direction of light ***i*** (or direction of uniaxial pressure ***m***) projection onto the X_1,X_2 plane and the X_1 axis (X_1, X_2, X_3 being the optical indicatrix axes). Indices *i, m* of θ and φ angles correspond to light polarization direction ***i*** and direction of uniaxial pressure ***m***, respectively.

This equation allows us to analyze the induced change of refractive index all over R^3 space under the influence of an applied uniaxial pressure along any direction ***m***(θ_m, φ_m) or the change of the refractive index along a chosen direction ***i***(θ_i, φ_i) under the influence of pressure ***m***(θ_m,φ_m) all over the R^3 space. For example, Fig. 1 represents some piezo-optic surfaces, as obtained by taking advantage of Eq. (7), for the case in which a uniaxial pressure is acting in three different directions (one for each panel in the figure) and light polarization ***i*** changes all over space (i.e. angles θ_i and φ_i span the R^3 space). Such surfaces are called ISs of light polarization [15, 29].

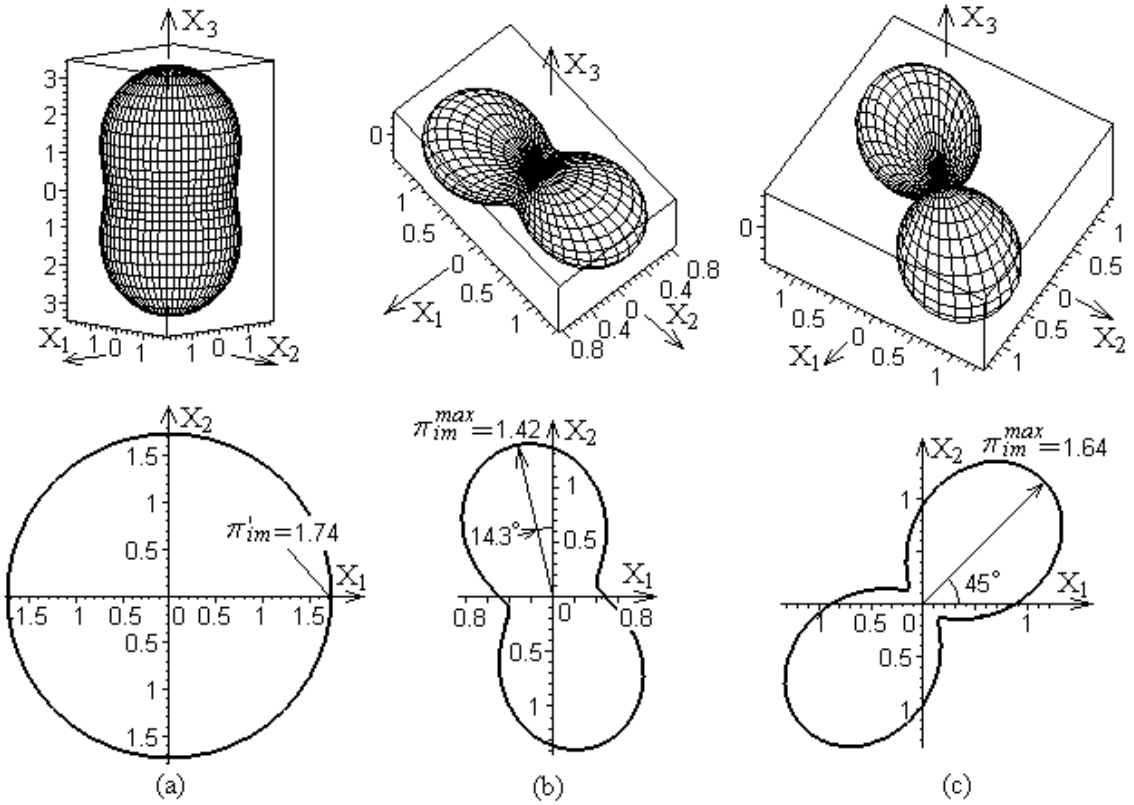

Fig. 1. POE indicative surfaces π'_{im} in $PbMoO_4$ crystals (all in Br) and their crosscuts in the main crystal physics plane X_1–X_2: (a) direction of uniaxial pressure $\boldsymbol{m} \parallel X_3$ ($\theta_m = 0^\circ$); (b) $\boldsymbol{m} \parallel X_1$ ($\theta_m = 90^\circ$, $\varphi_m = 0^\circ$); and (c) $\boldsymbol{m}$ is in the plane X_1–X_2 ($\theta_m = 90^\circ$) under angle $\varphi_m = 67.5^\circ$ with X_1. ISs are built by use of the π_{im} POC values reported in Table 2.

Fig. 1 clearly demonstrates that the maximum POE is achieved when $\boldsymbol{i} \parallel \boldsymbol{m} \parallel X_3$ that is, when $\theta_i = \theta_m = 0^\circ$. Indeed, by introducing these values for θ_i and θ_m into Eq. (7) one can reproduce the value of $\pi'_{im} = \pi_{33} = 3{,}34$ Br. The maximum value of the POE for other two surfaces (panels (b) and (c) of Fig. 1) is found in the X_1–X_2 plane along angles of 14º with respect to the X_2 axis and 45º with respect to either the X_1 or X_2 axes, respectively. These POE values (1.42 and 1.64 Br), however, are more than two times smaller than the maximum POC π_{33}.

Given that the directions of maximum POE in the isotropic X_1–X_2 plane coincide with the orientation of the semiaxes of the optical indicatrix, as perturbed by a uniaxial pressure, we can characterize the rotation of the optical indicatrix by an angle φ_i as induced by a pressure acting along the direction represented by angle φ_m in this plane. To do this, let us rewrite the equation for the POE surface given in Eq. (7) so as to consider its intersection with the X_1–X_2 plane ($\theta_i = 90^\circ$) in the case of a uniaxial pressure acting perpendicularly to the X_3 axis ($\theta_m = 90^\circ$). By introducing these mentioned values of the polar angles θ_m and θ_i into Eq. (7), we get:

$$\pi'_{im}(\varphi_i, \varphi_m) = (\pi_{11}\cos^2\varphi_m + \pi_{12}\sin^2\varphi_m + \frac{1}{2}\pi_{16}\sin 2\varphi_m)\cos^2\varphi_i + (\pi_{12}\cos^2\varphi_m + \pi_{11}\sin^2\varphi_m - \\ - \frac{1}{2}\pi_{16}\sin 2\varphi_m)\sin^2\varphi_i + (\pi_{61}\cos 2\varphi_m + \frac{1}{2}\pi_{66}\sin 2\varphi_m)\sin 2\varphi_i, \tag{8}$$

The directions along which the surface intersection represented by Eq. (8) exhibits minima and maxima can be determined by a partial derivative method $\partial\pi'_{im} / \partial\varphi_i = 0$. The solution in terms of angle φ_i gives:

$$\varphi_i = \frac{1}{2}\operatorname{arctg}\frac{2\pi_{61}\cos 2\varphi_m + \pi_{66}\sin 2\varphi_m}{(\pi_{11} - \pi_{12})\cos 2\varphi_m + \pi_{16}\sin 2\varphi_m}, \tag{9}$$

which provides the amplitude of the optical indicatrix rotation as a function of the direction along which the uniaxial pressure is acting. Interestingly, Eq. (9) demonstrates that the induced optical indicatrix rotation does not depend on the magnitude of the applied uniaxial pressure σ_m, but only on its direction (*via* the angle φ_m).

Figure 2, built on the basis of Eq. (9), shows that the optical indicatrix is not rotated ($\varphi_i = 0$) when the pressure is acting along the direction $\varphi_m = 8.8^\circ$. If $\varphi_m = 0^\circ$ that is, if the uniaxial pressure is acting along the X_1 axis, the indicatrix will be rotated by $\varphi_i = 14.3^\circ$, which is consistent with what reported in panel (b) of Fig. 1. Figure 3 further confirms these features as it reports the POE surface under the action of a uniaxial pressure along the direction $\varphi_m = 8{,}8^\circ$, where POE maxima and minima (and correspondingly the indicatrix axes) are found to coincide with the X_1 and X_2 axes.

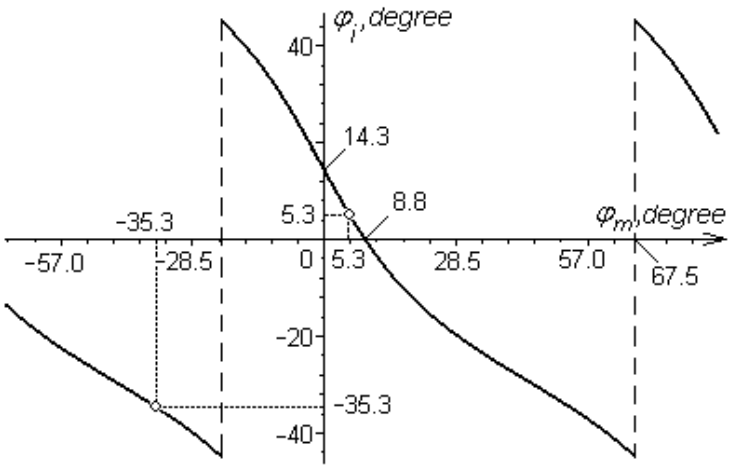

Fig. 2. Optical indicatrix rotation angle φ_i as a function of the direction of the uniaxial pressure (angle φ_m). Diamonds denote values where $\varphi_i = \varphi_m$ (i.e. when the direction of the indicatrix axes coincides with that of pressure action).

Let us now study the particular case in which the directions of pressure and POE maxima coincide that is, when $\varphi_m = \varphi_i$. For this purpose, φ_m in the rhs of Eq. (9) must be substituted by φ_i and the resulting equation be solved with respect to φ_i. In this case we obtain two solutions:

$$\varphi_i = \varphi_m = \frac{1}{2}\operatorname{arctg}\frac{(\pi_{12} - \pi_{11} + \pi_{66}) \pm \sqrt{(\pi_{11} - \pi_{12} - \pi_{66})^2 + 8\pi_{61}\pi_{16}}}{2\pi_{16}}. \qquad (10)$$

By introducing into Eq. (10) the π_{im} POC values from Table 2, we easily find that these angles are equal to −35,3º±90º and +5,3º±90º, which have been marked with a diamond in Fig. 2.

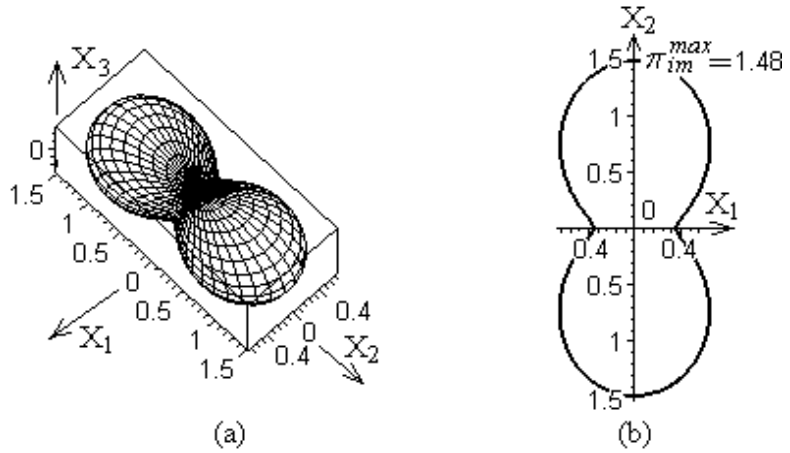

Fig. 3. POE surface under action of a uniaxial pressure along the direction φ_m = 8,8º (a) and its crosscut in the main plane X_1–X_2 (b).

We shall now consider some particular cases of surface (7): indicative surfaces of longitudinal and transverse piezo-optic effect. We refer to conditions of longitudinal POE when the directions of light polarization ***i*** and uniaxial pressure action ***m*** coincide with each other (i.e. when $\theta_m = \theta_i = \theta$ and $\varphi_m = \varphi_i = \varphi$). In this case, Eq. (7) then reduces to:

$$\pi'_{ii} = \pi_{11}\sin^4\theta(\sin^4\varphi + \cos^4\varphi) + \frac{1}{2}(\pi_{12} + \pi_{66})\sin^4\theta\sin^2 2\varphi + \frac{1}{4}(\pi_{13} + \pi_{31} + 2\pi_{44})\sin^2 2\theta + \\ + \pi_{33}\cos^4\theta + \frac{1}{4}(\pi_{16} + 2\pi_{61})\sin^4\theta\sin 4\varphi. \qquad (11)$$

This indicative surface is reported in Fig. 4 both in a 3D representation, panel (a), and in a 2D crosscut by the main X_1–X_2 plane, panel (b). The maximum value of this longitudinal POE indicative surface is found for $\theta = 0^\circ$ and corresponds to $\pi'_{ii} = \pi_{33} = 3.34$ Br. It follows that both surfaces (7) and (11) exhibit the same maximum value, which lay on the X_3 axis.

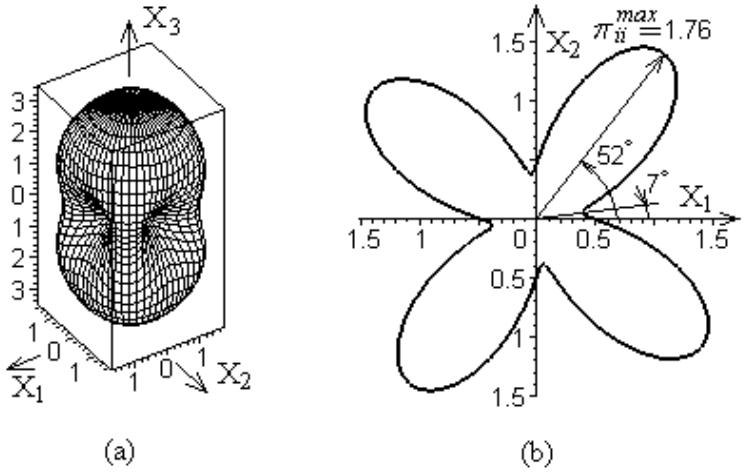

Fig. 4. Surface of longitudinal POE π'_{ii} (a) and its crosscut by the main plane X_1–X_2 (b).

When $\theta = 90^\circ$, Eq. (11) gives the crosscut of the longitudinal POE on the main X_1–X_2 plane:

$$\pi'_{ii} = \pi_{11}(\sin^4\varphi + \cos^4\varphi) + \frac{1}{2}(\pi_{12} + \pi_{66})\sin^2 2\varphi + \frac{1}{4}(\pi_{16} + 2\pi_{61})\sin 4\varphi. \quad (12)$$

This crosscut is reported in Fig. 4 (b). The directions along with this crosscut in the X_1–X_2 plane exhibts minima and maxima can be found by evaluating partial derivatives of Eq. (12) with respect to angle φ ($\partial\pi'_{ii} / \partial\varphi_i = 0$), which gives:

$$\varphi_{extr} = \frac{1}{4}\text{arctg}\left(\frac{\pi_{16} + 2\pi_{61}}{\pi_{11} - \pi_{12} - \pi_{66}}\right) \pm \frac{k\pi}{4}. \quad (13)$$

Angles $\varphi = 7^\circ \pm 90^\circ$ correspond to minima and $\varphi = 52^\circ \pm 90^\circ$ to maxima (with a value of $\pi'_{ii} = 1.76$ Br, which is almost two times lower than the value of maximum POC π_{33}).

We refer to the transverse piezo-optic effect when ***i*** and ***m*** directions are mutually perpendicular (i.e. $\theta_m = 90^\circ$, $\varphi_m = \varphi_i + 90^\circ$, for instance). By introducing these θ_m and φ_m values into Eq. (7) we get the indicative surface of light polarization:

$$\pi'^{(i)}_{im} = [\frac{1}{2}(\pi_{11} - \pi_{66})\sin^2 2\varphi_i + \pi_{12}(\cos^4\varphi_i + \sin^4\varphi_i) - \frac{1}{4}(\pi_{16} + 2\pi_{61})\sin 4\varphi_i]\sin^2\theta_i + \pi_{31}\cos^2\theta_i, \quad (14)$$

The corresponding crosscut by the main X_1–X_2 plane ($\theta_i = 90^\circ$) would be

$$\pi'^{(i)}_{im} = \frac{1}{2}(\pi_{11} - \pi_{66})\sin^2 2\varphi_i + \pi_{12}(\cos^4\varphi_i + \sin^4\varphi_i) - \frac{1}{4}(\pi_{16} + 2\pi_{61})\sin 4\varphi_i. \quad (15)$$

Surface (14) and its crosscut (15) are graphically represented in Fig. 5.

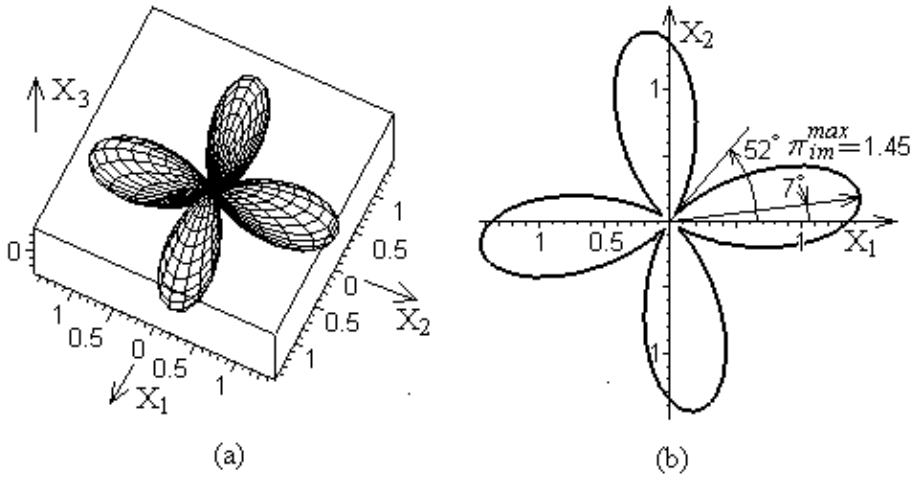

Fig. 5. Surface of transverse POE $\pi_{im}^{\prime(i)}$ (a) and its crosscut by the main plane X_1–X_2 (b).

We are not discussing this IS into detail given that its maximum values are significantly lower than the π_{33} POC. It should be noted, though, that φ_{extr} angles along which maximum and minimum values occur (see Fig.5) are very similar to those of the longitudinal POE (see Fig. 4) but where there is a maximum in the longitudinal there is now a minimum in the transverse and viceversa. Let us stress that other conditions referring to the transverse POE could be explored (such as $\theta_i = 90^\circ$, $\varphi_i = \varphi_m + 90^\circ$). Such a case corresponds to the mechanical stress indicative surface [15,29], whose equation for the 4/*m* symmetry class has been given in Ref. [7], and is characterized by a maximum value of the POE of about 1.5 Br.

3.3. Elasto-optic effect anisotropy

The equations for the indicative surfaces of longitudinal and transverse elasto-optic effect for crystals belonging to the 4/*m* symmetry class have already been reported [7]. Here, we just discuss into some detail the indicative surface of the longitudinal ELOE (i.e. for then ***i*** ∥ ***n*** where ***n*** is the strain direction) because it exhibits the maximum value of the elasto-optic effect. The corresponding equation takes the following form:

$$p'_{i^3} = p_{11}\sin^4\theta(\sin^4\varphi+\cos^4\varphi)+\frac{1}{2}(p_{12}+2p_{66})\sin^4\theta\sin^2 2\varphi+\frac{1}{4}(p_{13}+p_{31}+4p_{44})\sin^2 2\theta+ \\ +p_{33}\cos^4\theta+\frac{1}{2}(p_{16}+p_{61})\sin^4\theta\sin 4\varphi. \tag{16}$$

The intersection of this surface with the main X_1–X_2 plane is obtained by introducing the condition $\theta = 90^\circ$ into Eq. (16), which produces the next expression:

$$p'_{i^3} = p_{11}(\sin^4\varphi+\cos^4\varphi)+\frac{1}{2}(p_{12}+2p_{66})\sin^2 2\varphi+\frac{1}{2}(p_{16}+p_{61})\sin 4\varphi. \tag{17}$$

These two equations are graphically represented in Fig. 6, as evaluated by starting from the computed p_{in} coefficients reported in Table 2.

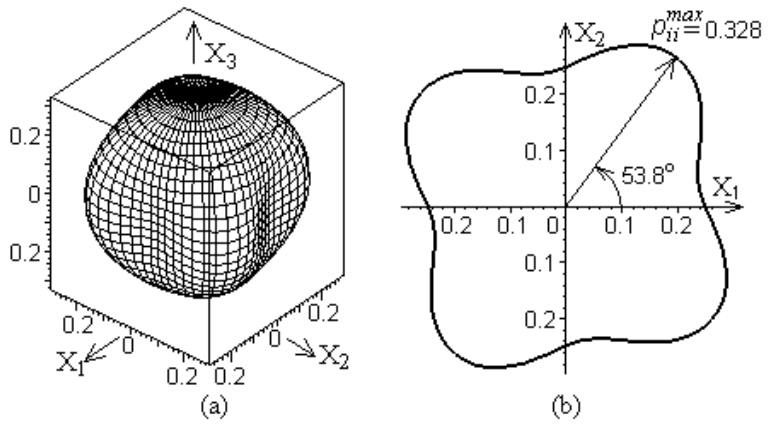

Fig. 6. Surface of longitudinal ELOE p'_{i3} (a) and its crosscut by the main plane X_1–X_2 (b).

The indicative surface for the longitudinal elasto-optic effect of Eq. (16) shows two large values. The first one corresponds to direction $\boldsymbol{i} \parallel \boldsymbol{n} \parallel X_3$, which is given by the spherical coordinate $\theta = 0^\circ$. By introducing this condition into Eq. (17), we would get $p'_{ii} = p_{33} = 0.318$. We shall now evaluate the acousto-optic efficiency associated with this ELOE value. The corresponding elasto-optic effect is caused by the longitudinal acoustic wave propagating along a direction parallel to the X_3 axis with a velocity $v = 3679$ m/s, as determined from the quantum-mechanically computed values of the elastic constants C_{mn} reported in Table 1 on the basis of Christoffel's equation [30]. It turns out that the coefficient of acousto-optic (AO) quality

$$M_2 = n_i^6 (p'_{ii})^2 / \rho v^3 \tag{18}$$

takes the value of $39 \cdot 10^{-15}$ s^3/kg, by considering the crystal density $\rho = 6950$ kg/cm^3. This simulated value of the M_2 AO quality coefficient for lead molibdate crystals is found to be in remarkable agreement with the corresponding experimental value of $36 \cdot 10^{-15}$ s^3/kg [3,31], within the typical range of errors of elasto-optic effect experimental studies (differences among p_{in} values as experimentally determined in different studies were given in Table 2), which confirms the reliability of the quantum-mechanical method [12,13] here adopted for the determination of all elasto-optic coefficients. The second large ELOE value ($p'_{ii} = 0.328$) occurs in the X_1–X_2 plane at an angle $\varphi = 53.8^\circ$ with respect to the axis X_1 [see Fig. 6, panel (b)]. The velocity of the longitudinal acoustic wave along this direction is large ($v = 4355$ m/s) and thus makes the M_2 coefficient smaller ($34.6 \cdot 10^{-15}$ s^3/kg). Other geometries of acousto-optic interaction are characterized by even smaller M_2 values.

To summarize, the maximum value of the AO quality coefficient M_2 in $PbMoO_4$ crystals corresponds to a simple condition of AO interaction (i.e. to a longitudinal acoustic wave propagating along the X_3 axis and to light polarization direction $\boldsymbol{i} \parallel X_3$), which agrees with the determination by Pinnow [3]. On the other hand, it has been shown, on the basis of ELOE anisotropy analysis in $CaWO_4$, SrB_4O_7 and GaP crystals [6,7,15], that the maximum value of the M_2 coefficient can occur for directions of acoustic wave propagation not coinciding with the main crystal physics axes. For this reason, the study of the anisotropy of the elasto-optic effect is required in order to determine the conditions for the largest acousto-optic efficiency of new crystals.

4. Conclusions

Quantum-mechanical simulations, based on the density-functional-theory, have been performed to determine all the components of the forth-rank elastic, compliance, photo-elastic and piezo-optic tensors of lead molibdate $PbMoO_4$ crystals. It has been shown that lead molibdate enables a high piezo-optic efficiency with a maximum change of the specimen optical path (per unit of mechanical stress and specimen length) of 24.9 Br, which is a much larger value than for other piezo-optic materials such as $LiNbO_3$, $CaWO_4$ or GaP.

In many crystals (such as $CaWO_4$, SrB_4O_7, GaP) the directions along which acoustic waves are propagated with the maximum acousto-optic efficiency do not necessarily coincide with the main crystal physics axes. It follows that, in order to determine the optimal conditions for the acousto-optic interaction, the anisotropy of the elasto-optic and piezo-optic effects must be explicitly investigated. Indicative surfaces of the piezo-optic and elasto-optic effects of lead molibdate have been investigated and their maximum values found, which have allowed to determine the value of the acousto-optic quality coefficient M_2 ($39 \cdot 10^{-15}$ s^3/kg). The conditions for the most effective acousto-optic interaction in $PbMoO_4$ crystals have been confirmed to be such that the directions of longitudinal acoustic wave propagation and light wave polarization are both oriented along the X_3 crystal optical axis.

It has also been determined that the induced rotation of the optical indicatrix in the X_1–X_2 plane under the action of an applied uniaxial pressure can be very large (up to tens of degrees) and depends on uniaxial pressure direction rather than magnitude, which should be properly taken into account when designing acousto-optic cells.

REFERENCES

1. M.P. Shaskolskaya et al., *Acoustic crystals. Handbook* (Moscow: Nauka, 1982).
2. G. A. Coquin, D. A. Pinnow, and A. W. Watner, "Physical properties of lead molybdate relevant to acousto-optic device applications," J. Appl. Phys. **42,** 2162–2168 (1971).
3. D. A. Pinnow, L. G. Van Uitert, A. W. Warner, and W. A. Bonner, "Lead molybdate: a melt-grown crystal with a high figure of merit for acousto-optic device applications," Appl. Phys. Lett. **15**, 83–86 (1969).
4. V. T. Gabrielyan, V. V. Kludzin, S. V. Kulakov, and B. P. Razzhivin, "Elastic and photoelastic properties of lead molibdate monocrystals," Solid State Physics **17,** 603–605 (1975) [in Russian].
5. V. V. Badikov, S. V. Bogdanov, A. A. Godovikov, I. I. Zubrinov, and D. V. Sheloput, "Proustite monocrystals as a material for acousto-optic devices," Acoustic journal **17**, 300–301 (1971) [in Russian].
6. N. M. Demyanyshyn, B. G. Mytsyk, and O. M. Sakharuk, "Elasto-optic effect anisotropy in strontium borate crystals," Appl. Opt. **53**, 1620–1628 (2014).
7. N. M. Demyanyshyn, B. G. Mytsyk, Ya. P. Kost', I. M. Solskii, and O. M. Sakharuk, "Elasto-optic effect anisotropy in calcium tungstate crystals," Appl. Opt. **54**, 2347–2355 (2015).
8. M. N. Trainer, "Photoelastic measuring transducer and accelerometer based thereon," Patent US 4.648.274 (1987).
9. F. Brandi, E. Polacco, and G. Ruoso, "Stress-optic modulator," Meas. Sci. Technol. **12**, 1503–1508 (2001).
10. F. Bammer, J. Petelin, R. Petkovsek, "Measurements on a single crystal photoelastic modulator," Conference publications, Lasers and electro-optics conference, 1-6 May 2011, Baltimore, USA, 1–2 (2011).
11. A. S. Andrushchak, B. G. Mytsyk, and B. V. Osyka, "Photoelastic pressure transducer," USSR Author's certificate 1796936 (1993) [in Russian].
12. A. Erba and R. Dovesi, "Photoelasticity of crystals from theoretical simulations", Phys. Rev. B **88**, 045121 (2013).
13. A. Erba, M. T. Ruggiero, T. M. Korter, and R. Dovesi, "Piezo-optic tensor of crystals from quantum-mechanical calculations," J. Chem. Phys. **143**, 144504/1–8 (2015).
14. R. Dovesi, R. Orlando, A. Erba, C. M. Zicovich-Wilson, B. Civalleri, S. Casassa, L. Maschio, M. Ferrabone, M. De La Pierre, Ph. D'Arco, Y. Noël, M. Causà, M. Rérat, and B. Kirtman, "CRYSTAL14: A program for the ab initio investigation of crystalline solids," Int. J. Quant. Chem. **114**, 1287–1317 (2014).
15. B. G. Mytsyk, N. M. Demyanyshyn, and O. M. Sakharuk, "Elasto-optic effect anisotropy in gallium phosphide crystals," Appl. Opt. **54**, 8546–8553 (2015).
16. A. Erba, A. Mahmoud, R. Orlando and R. Dovesi, "Elastic properties of six silicate garnet end-members from accurate ab initio simulations", Phys. Chem. Minerals 41, 151-160 (2014).

17. C. Adamo and V. Barone, “Toward reliable density functional methods without adjustable parameters: The PBE0 model”, J. Chem. Phys. **110**, 6158 (1999).
18. A. Erba, Kh. E. El-Kelany, M. Ferrero, I. Baraille and M. Rérat, “Piezoelectricity of $SrTiO_3$: An ab initio description.” Phys. Rev. B, **88**, 035102 (2013).
19. A. Mahmoud, A. Erba, Kh. E. El-Kelany, M. Rérat and R. Orlando, “Low-temperature phase of $BaTiO_3$: Piezoelectric, dielectric, elastic and photoelastic properties from ab initio simulations” Phys. Rev. B, **89**, 045103 (2014).
20. E. Heifets, E. A. Kotomin, A. A. Bagaturyants and J. Maier, “Ab Initio Study of $BiFeO_3$: Thermodynamic Stability Conditions” J. Phys. Chem. Lett. **6** 2847-2851 (2015).
21. D. Zagorac, K. Doll, J. C. Schoen, and M. Jansen, “Ab initio structure prediction for lead sulfide at standard and elevated pressures”, Phys. Rev. B **84**, 045206 (2011)
22. F. Corà , A. Patel, N.M. Harrison, C. Roetti and C.R.A. Catlow, “An ab-initio Hartree-Fock study of alpha-MoO_3”, J. Mater. Chem. **7**, 959-967 (1997).
23. J. M. Farley, G. A. Saunders, and D. Y. Chung, “Elastic properties of scheelite structure molybdates and tungstates,” J. Phys. C: Sol. State Phys. 8, 780–786(1975).
24. B. Mytsyk, “Methods for the studies of the piezo-optical effect in crystals and the analysis of experimental data. Part I. Methodology for the studies of piezooptical effect,” Ukr. J. Phys. Opt. **4**/1, 1–26 (2003).
25. B. G. Mytsyk, *Photoelasticity of Anisotropic Materials* (Liga-press, 2012) [in Ukrainian].
26. B. G. Mytsyk, A. S. Andrushchak, N. M. Demyanyshyn, Y. P. Kost’, A. V. Kityk, P. Mandracci, and W. Schranz, “Piezo-optic coefficients of MgO-doped $LiNbO_3$ crystals,” Appl. Opt. **48**, 1904–1911 (2009).
27. B. G. Mytsyk, Ya. P. Kost’, N. M. Demyanyshyn, A. S. Andrushchak, and I .M. Solskii, “Piezo-optic coefficients of $CaWO_4$ crystals,” Crystallogr. Rep. **60**, 130–137 (2015).
28. B. G. Mytsyk, A. S. Andrushchak, and Y. P. Kost’, “Static photoelasticity of gallium phosphide crystals,” Crystallogr. Rep. **57**, 124–130 (2012).
29. B. G. Mytsyk and N. M. Demyanyshyn, “Piezo-optic surfaces of lithium niobate crystals,” Crystallogr. Rep. **51**, No. 4, 653–660 (2006).
30. T. S. Narasimhamurty, *Photoelastic and Electrooptic Properties of Crystals* (Plenum, 1981).
31. M. J. Weber, *Handbook of optical materials* (CRC Press, 2003).